MBOAT7 and CDS2 coordinate lipid droplet dynamics and cholesterol metabolism in liver

Jiesi Xu[1, 2, 3, *], Jianxin Zhang[3, 4, *], Wei Wang[3], Honggang Su[3, 4], Siyu Chen[5], Mei Ding[2, 3] and Xun Huang[2, 3, 6, #]

1. The Key Laboratory of Geriatrics, Beijing Institute of Geriatrics, Institute of Geriatric Medicine, Chinese Academy of Medical Sciences, Beijing Hospital/National Center of Gerontology of National Health Commission, Beijing, 100730, China

2. State Key Laboratory of Metabolism and Regulation in Complex Organisms, Taikang Center for Life and Medical Sciences, School of Basic Medical Sciences, Wuhan University, Wuhan, Hubei 430071, China

3. Institute of Genetics and Developmental Biology, Chinese Academy of Sciences, Beijing 100101, China

4. University of Chinese Academy of Sciences, Beijing 100049, China

5. Medical Research Center, Beijing Institute of Respiratory Medicine and Beijing Chao-Yang Hospital, Capital Medical University, Beijing 100020, China

6. Tianjian Laboratory of Advanced Biomedical Sciences, Zhengzhou University, Zhengzhou 450001, China

* Equal contribution

To whom correspondence should be addressed at: State Key Laboratory of Metabolism and Regulation in Complex Organisms, Taikang Center for Life and Medical Sciences, School of Basic Medical Sciences, Wuhan University, Wuhan, Hubei 430071, China

Email: huangxun@whu.edu.cn; xhuang@genetics.ac.cn

Abstract

Metabolic dysfunction-associated steatotic liver disease (MASLD) is a highly prevalent disorder worldwide characterized by the accumulation of hepatic lipid droplets (LDs). However, the mechanisms by which hepatocytes adapt to the dynamic changes in LD morphology to maintain metabolic homeostasis remains poorly understood. Here, we show that MBOAT7, a known MASLD-associated protein, cooperates with CDS2 to regulate lipid droplet dynamics and cholesterol metabolism. Under physiological conditions, their interaction in the endoplasmic reticulum (ER) maintains metabolic homeostasis. Disruption of this interaction, such as through CDS2 knockdown or loss of function, triggers an adaptive response wherein MBOAT7 translocates to ER-LD contact sites in a RAB1-dependent manner. This redistribution reduces LD size and activates the AMPK signaling, thereby promoting cholesterol excretion. Conversely, impairment of this compensatory axis results in hepatic cholesterol accumulation, a key driver of MASLD progression. Our findings uncover a mechanism that integrates inter-organelle communication with metabolic regulation, offering new insights into MASLD pathogenesis.

Introduction

Metabolic dysfunction-associated steatotic liver disease (MASLD) has emerged as the most prevalent chronic liver disorder worldwide, affecting 20%-25% of the general population (1, 2). Despite its significant clinical burden, the mechanisms that drive disease onset and progression remain incompletely understood, limiting the development of effective therapeutic strategies.

A central hallmark of MASLD is the excessive accumulation of hepatic lipid droplets (LDs), dynamic organelles that function as central hubs for neutral lipid storage and metabolism (3). Under pathological conditions, hepatocyte LDs can undergo substantial expansion in size, leading to macrovesicular steatosis. In response to lipid overload, hepatocytes can adapt by remodeling LD morphology toward small LDs. This shift is generally considered protective, as smaller LDs present a larger surface area-to-volume ratio and are more accessible for lipolysis and lipophagic degradation (4). Nevertheless, while small LDs are more metabolically active and facilitate lipid mobilization, their persistence can also increase the generation of lipotoxic intermediates. To mitigate potential lipotoxicity from sustained LD turnover, hepatocytes employ several compensatory mechanisms, such as directing free fatty acids toward oxidation, re-esterification, or export. Moreover, this adaptive process involves active remodeling of inter-organelle contacts between LDs and other organelles—such as the endoplasmic reticulum, mitochondria, and lysosomes—further integrating lipid handling with cellular metabolic homeostasis. Thus, LD remodeling represents a crucial adaptive process for maintaining hepatic metabolic homeostasis. Although LD-associated proteins are known to modulate LD size, their specific roles during the adaptive phase of hepatic steatosis are not fully understood.

The MBOAT7 (membrane-bound O-acyltransferase 7) variant rs641738 (C>T, loss of function mutation) has been robustly linked to all stages of MASLD, including steatosis, inflammation and fibrosis (5-8). MBOAT7 catalyzes the incorporation of arachidonic acid into phosphatidylinositol (PI) through the PI remodeling Lands' cycle (9). Parallel to this pathway, PI can also be synthesized *de novo* via the Kennedy

76 pathway, in which the conversion of phosphatidic acid to CDP-diacylglycerol
77 (CDP-DAG) by CDS (CDP-DAG synthase) constitutes a critical step (9, 10). Notably,
78 CDS2, one of the two CDS proteins in mammals, is selectively inhibited by
79 arachidonoyl-containing PI species (PI-AA), suggesting a regulatory feedback loop
80 that links MBOAT7-mediated PI remodeling with CDS2-mediated *de novo* PI
81 synthesis (11). This interplay is biologically significant: *Mboat7* deficiency has been
82 shown to promote hepatic lipid accumulation and steatohepatitis, partly through
83 increasing CDS2 activity (12, 13). Conversely, deletion of *Cds2* leads to the formation
84 of large LDs and spontaneous development of metabolic dysfunction-associated
85 steatohepatitis (MASH) (14-16), providing a valuable model for studying hepatocyte
86 adaptations to drastic LD morphological changes. Although MBOAT7 has been
87 implicated in modulating LD lipid composition (13, 17), its precise subcellular
88 localization and functional relationship with CDS2 in regulating LD dynamics remain
89 unclear.
90 Here, we uncover a coordinated mechanism in which MBOAT7 and CDS2 jointly
91 regulate LD dynamics and cholesterol metabolism. We show that deletion of CDS2
92 results in adaptive relocation of MBOAT7 to ER-LD contact sites via RAB1, where it
93 restricts LD expansion and activates the AMPK-LXR axis to promote cholesterol
94 excretion, thereby protecting hepatocytes from lipotoxicity. Conversely, disruption of
95 this regulatory circuit leads to cholesterol accumulation-a central feature of MASLD
96 progression. These findings establish MBOAT7 and CDS2 as key regulators of a
97 membrane-metabolic crosstalk that integrates inter-organelle communication with
98 metabolic control, revealing a robust metabolic adaptation to hepatic steatosis in
99 hepatocytes.
100
101 **Results**
102 **MBOAT7 and CDS2 regulate cholesterol and fatty acid metabolism in liver**
103 To investigate the connection between MBOAT7 and CDS2, we analyzed hepatic
104 transcriptome datasets and GEPIA (Gene Expression Profiling Interactive Analysis).
105 This showed that *MBOAT7* and *CDS2* expression levels in human liver samples are

106 positively correlated (Figure 1A-C). Both *MBOAT7* and *CDS2* are upregulated in liver
107 tumor samples compared with non-tumor liver samples (Figure S1A). To determine
108 the roles of MBOAT7 and CDS2 in the regulation of hepatic lipid metabolism, we
109 specifically knocked down these enzymes in the liver by injecting C57BL/6 mice with
110 AAV-TBG-sh*Mboat7*, AAV-TBG-sh*Cds2* or
111 AAV-TBG-sh*Mboat7*+AAV-TBG-sh*Cds2* (Figure 1D). Consistent with previous
112 report (18), knockdown of *Mboat7* in liver did not affect plasma lipid content but
113 increased hepatic triglyceride and cholesterol content (Figure 1E-F and Figure S1B-C).
114 Knockdown of *Cds2* did not affect plasma triglyceride content, but increased plasma
115 and hepatic cholesterol and hepatic triglyceride content (Figure 1E-F and Figure
116 S1B-C). Knockdown of both *Mboat7* and *Cds2* did not further enhance triglyceride
117 and cholesterol content (Figure 1E-F and Figure S1B-C), indicating that combined
118 knockdown of *Mboat7* and *Cds2* did not exert additive effects on the increased lipid
119 levels. Consistent with the above results, H&E staining showed that knockdown of
120 *Mboat7*, *Cds2*, and *Mboat7* + *Cds2* increased hepatic steatosis (Figure 1G-H).
121 To examine the pathways regulated by MBOAT7 and CDS2, we performed RNA
122 sequencing (RNAseq) analysis on liver from the sh*Mboat7*, sh*Cds2*, and sh*Mboat7* +
123 sh*Cds2* groups. When we compared the results, we noticed an extensive overlap
124 between the three datasets: 266 genes were significantly upregulated and 301 genes
125 were significantly downregulated in all three groups (Figure 1I). Kyoto Encyclopedia
126 of Genes and Genomes (KEGG) analysis revealed significant changes in cholesterol
127 and fatty acid metabolism pathways among the genes with downregulated expression
128 in all three groups (Figure 1J). For the genes with upregulated expression in all three
129 groups, KEGG analysis revealed significant alterations in steroid biosynthesis and
130 non-alcoholic fatty liver pathways (Figure S1D). LXR, a key regulator of cholesterol
131 efflux, controls the transcription levels of genes such as *Abca1* and *Abcg5/8*. Our
132 qPCR analysis showed that genes involved in cholesterol excretion (*Lxr, Abcg8* and
133 *Abca1*) were downregulated in liver (Figure 1K), indicating that reduced expression
134 of *Mboat7* or *Cds2* impairs cholesterol excretion. Knockdown of *Mboat7* and *Cds2*
135 increased the expression of *Fasn*, which regulates fatty acid biosynthesis (Figure 1K).

136 Accordingly, LXR protein levels were reduced in the liver of sh*Mboat7*, sh*Cds2*, and
137 sh*Mboat7*+sh*Cds2* mice (Figure 1L and Figure S1E). Nuclear SREBP2 and HMGCR
138 levels were diminished, likely due to feedback inhibition of cholesterol biosynthesis
139 by increased cellular cholesterol levels (Figure 1L and Figure S1E). ALT and AST
140 measurements revealed that knockdown of *Mboat7* or *Cds2* or both did not exacerbate
141 liver inflammation (Figure S1F and G). Overall, these data suggests that MBOAT7
142 and CDS2 coordinate fatty acid and cholesterol metabolism.
143
144 **MBOAT7 is localized to the ER-LD contacts in lipid-loaded CDS2 KO cells**
145 To investigate how MBOAT7 and CDS2 cooperatively regulate lipid metabolism, we
146 focused on LDs. Previous studies have shown that CDS2 knockout increases LD size
147 (15). We examined the localization and roles of MBOAT7 in LD regulation.
148 MBOAT7-EGFP exhibited an ER-like localization pattern in both wild-type and
149 CDS2 KO HeLa cells (Figure S2A and B). Interestingly, in CDS2 KO cells treated
150 with oleic acid (OA) to induce LD formation, MBOAT7-EGFP (Figure 2A-B) and
151 MBOAT7-mCherry (Figure S2C-D) surrounded LDs stained by LipidTOX and
152 BODIPY, respectively. In contrast, MBOAT7-EGFP did not show colocalization with
153 LDs in OA-treated control HeLa cells (Figure 2A-B). Furthermore, in OA-treated
154 CDS2 KO cells, MBOAT7-EGFP was colocalized with the LD marker
155 mScarlet-PLIN1, whereas no such colocalization was observed in control cells
156 (Figure S2E). Similarly, in OA-treated HepG2 cells, MBOAT7-EGFP remained
157 localized to the ER, but enclosed LDs when CDS2 was knocked down (Figure S2F).
158 We also analyzed the localization of endogenous MBOAT7. In OA-treated CDS2 KO
159 cells, endogenous MBOAT7 colocalized with LDs, but this was not observed in
160 OA-treated control cells (Figure 2C-D). 3D reconstruction of the LD surface
161 confirmed that MBOAT7 localized to the LD surface in OA-treated CDS2 KO cells
162 (Figure 2E). Since MBOAT7 is a multipass transmembrane protein, it is likely
163 localized to the ER regions adjacent to LDs, rather than to the LD membrane.
164 The colocalization of MBOAT7 with LDs in CDS2 KO cells led us to test
165 whether CDS2 depletion affects the targeting of other ER proteins to LDs. The ER

166 marker mScarlet-SEC61b did not colocalize with LDs in OA-loaded CDS2 KO cells
167 (Figure 2F-G). Since CDS2 protein levels are downregulated in MASLD mouse
168 models (16), we also tested whether MBOAT7 targets to LDs in the liver of MASLD
169 model mice, in which MASLD is induced by the feeding with the
170 fat/fructose/cholesterol-rich Gubra-Amylin NASH (GAN) diet. Confocal imaging
171 showed that endogenous MBOAT7 was more enriched at the LD periphery in liver
172 sections from GAN diet-induced MASLD mice compared to those from normal mice
173 (Figure 2H-I). These findings suggest that MBOAT7 specifically localizes to the
174 ER-LD contacts in lipid-overloaded CDS2-deficient cells but not in control cells.
175

176 **The N-terminus of MBOAT7 is required for localization of MBOAT7 to ER-LD**
177 **contacts in CDS2 KO cells**

178 MBOAT7 consists of 11 transmembrane (TM) helices organized into two bundles
179 (TM1-5 and TM9-11) that tilt apart, creating a central catalytic chamber (19) (Figure
180 3A). To identify the region required for the localization of MBOAT7 to ER-LD
181 contacts, we generated three EGFP-tagged truncated versions of MBOAT7,
182 containing the N-terminal region (amino acids 1-135), the central region (180-310),
183 and the C-terminal region (311-472) (Figure 3A). Only the N-terminal region
184 localized to ER-LD contacts in CDS2 KO cells, and MBOAT7 with a deletion of the
185 N-terminal 99 amino acids did not localize to ER-LD contacts (Figure 3B). We further
186 investigated the specific TM regions critical for LD targeting in CDS2 KO cells.
187 Deleting TM1-2 slightly disrupted MBOAT7's ring-like pattern on LDs, while
188 deleting TM3-4 completely abolished its LD anchoring (Figure 3C). To validate the
189 importance of TM3-4 for ER-LD localization, we generated chimeric proteins by
190 swapping TM3 or TM4 with the corresponding regions from MBOAT5, which
191 belongs to the membrane-bound O-acyltransferase (MBOAT) family and carries out
192 re-acylation of phosphatidylserine (PS) and phosphatidylcholine (PC) on ER.
193 MBOAT7 and MBOAT5 have similar structure (19). These chimeric proteins failed to
194 localize to LDs (Figure 3D). Therefore, the N-terminus of MBOAT7, particularly
195 TM3-4, is required for the localization of MBOAT7 to ER-LD contacts in CDS2 KO

196 cells.

197

198 **MBOAT7 interacts with CDS2**

199 Next, we examined why MBOAT7 is localized to the ER-LD contacts in CDS2 KO
200 cells but not in control cells. Similar to MBOAT7, CDS2 is localized to the ER and
201 MAMs (16). We hypothesized that CDS2 retains MBOAT7 at the ER, while
202 MBOAT7 relocates to the ER-LD contacts in the absence of CDS2.
203 Co-immunoprecipitation (co-IP) assays demonstrated that Flag-CDS2 precipitated
204 MBOAT7-EGFP (Figure 3E), and conversely, MBOAT7-EGFP precipitated
205 Flag-CDS2 (Figure 3F). Using CRISPR-based knock-in (KI) of EGFP at the
206 N-terminus of endogenous CDS2, we found that endogenous CDS2 coprecipitated
207 with endogenous MBOAT7 (Figure 3G). To examine the direct binding between these
208 two proteins, we purified His-MBOAT7 from *E. coli* and Flag-CDS2 from
209 mammalian cells. Western blot analysis confirmed their direct interaction (Figure 3H).
210 Overall, these results indicate that CDS2 interacts with MBOAT7, retaining it at the
211 ER.

212

213 **RAB1 is required for localization of MBOAT7 at ER-LD contacts in CDS2 KO**
214 **cells**

215 Next, we investigated how MBOAT7 targets to the ER-LD contacts in CDS2 KO cells.
216 ER proteins typically target the LD monolayer surface, which requires membrane
217 continuity between the ER outer leaflet and the LD monolayer (20). This targeting can
218 occur either during early LD formation or to mature LDs after their formation. These
219 ER proteins associate with the LD monolayer through hydrophobic hairpins, which
220 insert midway into the lipid bilayers of the ER, with both the N- and C-termini facing
221 the cytosol (21). MBOAT7, however, is a multispanning transmembrane protein with
222 11 transmembrane domains, making it unlikely that MBOAT7 localizes directly to the
223 LD monolayer. Since MBOAT7 lacks a hairpin structure, we hypothesized that
224 ER-localized MBOAT7 associates with LDs in CDS2 KO cells via interaction with
225 LD-associated proteins.

226 We immunoprecipitated MBOAT7-EGFP from control and CDS2 KO cells and
227 identified its interacting proteins using LC-MS/MS (Figure 4A). We hypothesized that
228 MBOAT7 would interact with LD proteins in CDS2 KO cells but not in control cells,
229 so we selected candidates whose interaction with MBOAT7 in CDS2 KO cells was at
230 least 2-fold stronger than in control cells. Based on previously published LD
231 proteomes (22-24), we focused on LD proteins. Five proteins from our dataset were
232 shared with all the published LD proteomes (Figure 4B). Interestingly, of these five
233 candidates, four of them are RAB proteins (RAB1A, RAB7A, RAB14 and RAB18)
234 (Figure 4C). RAB1 mediates targeting triglyceride biosynthetic enzymes to LDs (25,
235 26). Our results showed that knockdown of RAB1A impaired the LD targeting of
236 MBOAT7 in OA-loaded CDS2 KO cells (Figure 4D-F). Co-IP assays showed that
237 MBOAT7-EGFP interacted with Flag-RAB1A in CDS2 KO cells but not in control
238 cells, suggesting that RAB1A helps MBOAT7 target to the ER-LD contacts in CDS2
239 KO cells (Figure 4G). Furthermore, expressing HA-tagged CDS2 in CDS2 KO cells
240 inhibited the interaction between MBOAT7 and RAB1A (Figure 4H). Together, these
241 results suggest that RAB1A is essential for targeting of MBOAT7 to the ER-LD
242 contacts in CDS2 KO cells, and that CDS2 inhibits this targeting by competing with
243 RAB1A for binding to MBOAT7.
244
245 **MBOAT7 reduces LD size in CDS2 KO cells by inhibiting the targeting of**
246 **DGAT2 to LDs**
247 We next investigated the cellular and physiological functions of ER-LD
248 contact-localized MBOAT7. Overexpression of MBOAT7-EGFP did not affect LD
249 size in control cells, but it reduced LD size in CDS2 KO cells (Figure 5A-B).
250 Overexpression of an MBOAT7 mutant with reduced catalytic activity
251 (MBOAT7(N321A, H356A)-EGFP) still reduced the LD size in CDS2 KO cells
252 (Figure 5A-B). This indicates that the effect of MBOAT7 on LD size reduction in
253 CDS2 KO cells is independent of its enzymatic activity.
254 To explore the underlying mechanism, we considered previous findings
255 suggesting that the lipid biosynthetic enzymes DGAT2 and GPAT4 target LDs earlier

256 in CDS2 KO cells than in control cells, promoting LD growth (14). Knockdown of
257 DGAT2 or GPAT4 reduced the LD size in CDS2 KO cells (14). We hypothesized that
258 MBOAT7 may impede the LD targeting of DGAT2 or GPAT4 by competitively
259 interacting with RAB1, thus limiting LD growth in CDS2 KO cells. Consistent with
260 this idea, we found that both Flag-DGAT2 and Flag-GPAT4 bound to GFP-tagged
261 RAB1A (Figure 5C and D). The interaction between GPAT4 and RAB1A was
262 unaffected by MBOAT7 overexpression (Figure S3A). Importantly, MBOAT7-EGFP
263 expression reduced the binding between Flag-DGAT2 and GFP-RAB1A in CDS2 KO
264 cells (Figure 5E). Conversely, knockdown of MBOAT7 enhanced the binding between
265 Flag-DGAT2 and GFP-RAB1A in CDS2 KO cells (Figure 5F). Confocal images
266 showed that EGFP-DGAT2 was targeted to LDs in CDS2 KO cells, but
267 overexpression of MBOAT7-mCherry blocked this targeting (Figure 5G). Both
268 Flag-DGAT2 and Flag-MBOAT7 interact with full-length GFP-RAB1A. However,
269 their interactions are markedly reduced when RAB1A is truncated at either the
270 N-terminus or the C-terminus (Figure 5H-I). In response to OA treatment, triglyceride
271 synthesis enzymes like DGAT2 or GPAT4 are more likely to target to LDs to promote
272 LD growth (27). Since this process requires RAB1, we then tested whether OA
273 treatment affects the interaction of these enzymes with RAB1. OA treatment enhanced
274 DGAT2 binding to RAB1A but did not affect GPAT4 binding to RAB1A (Figure 5J
275 and Figure S3B). Interestingly, MBOAT7 binding to RAB1A increased after OA
276 treatment in CDS2 KO cells (Figure 5K). Taken together, our data suggest that CDS2
277 retains MBOAT7 at the ER. When CDS2 is absent, MBOAT7 binds to RAB1 and
278 localizes to the ER-LD contacts. Furthermore, MBOAT7 reduces the size of LDs by
279 inhibiting the targeting of DGAT2 to LDs.
280
281 **MBOAT7 regulates LD size and lipolysis in the absence of CDS2**
282 The studies above reveal the regulatory roles of MBOAT7 and CDS2 in controlling
283 LD size in cultured cells. We next examined how MBOAT7 and CDS2 functionally
284 interact and regulate LD size *in vivo*. Since MBOAT7 and CDS2 are bound to each
285 other, we tested whether CDS2 affects the acyltransferase activity of MBOAT7 using

286 MBOAT7 substrates like lyso-PI and [14C]-arachidonic acid. We analyzed the activity
287 of MBOAT7 in the liver from control mice (*Cds2*$^{f/f}$), mice with liver-specific depletion
288 of CDS2 (*Cds2*$^{f/f}$*;AlbCre*), and hepatic CDS2-depleted mice with AAV-mediated
289 hepatic re-expression of CDS2 (*Cds2*$^{f/f}$*;AlbCre* + AAV-CDS2). The results showed
290 that CDS2 deficiency did not significantly impact the enzymatic activity of MBOAT7
291 (Figure 6A).

292 To determine how MBOAT7 and CDS2 regulate LDs *in vivo*, *Cds2*$^{f/f}$ and
293 *Cds2*$^{f/f}$*;AlbCre* mice were injected with AAV-TBG-Con or AAV-TBG-*Mboat7* (Figure
294 6B). Hepatic overexpression of *Mboat7* did not affect plasma lipids in either control
295 or *Cds2*$^{f/f}$*;AlbCre* mice (Figure S4A-B). Hepatic overexpression of *Mboat7* did not
296 change hepatic triglyceride and cholesterol levels in *Cds2*$^{f/f}$ mice, but it reduced
297 hepatic cholesterol levels in *Cds2*$^{f/f}$*;AlbCre* mice (Figure 6C and D). H&E staining
298 showed that liver sections from *Cds2*$^{f/f}$*;AlbCr*e mice contained "supersized" LDs,
299 while overexpression of *Mboat7* reduced the LD size in *Cds2*$^{f/f}$*;AlbCre* mice, resulting
300 in multiple small-sized LDs in hepatocytes (Figure 6E). This reduction in LD size was
301 also confirmed in *Cds2*-deficient primary hepatocytes (Figure 6F and G). Cell
302 fractionation assays revealed that overexpression of *Mboat7* reduced the protein level
303 of DGAT2 in the LD fraction from the livers of *Cds2*$^{f/f}$*;AlbCre* mice, while increasing
304 the protein level of ATGL (also called PNPLA2) (Figure 6H), a rate-limiting enzyme
305 for lipolysis. To test if MBOAT7 regulates lipolysis, we used isoprenaline (ISO) to
306 stimulate lipolysis. The results showed that overexpression of MBOAT7 increased
307 free fatty acid (FFA) release in both DMSO and ISO-treated *Cds2*-deficient primary
308 hepatocytes (Figure 6I).

309 Overall, our data suggest that MBOAT7 controls LD size and lipolysis by
310 inhibiting DGAT2 targeting to LDs and promoting ATGL targeting to LDs in both
311 CDS2-deficient cell lines and primary hepatocytes.

312

313 **MBOAT7 and CDS2 regulate cholesterol metabolism through the AMPK**
314 **pathway**

315 We next investigated the physiological significance of ER-LD contact-localized

316 MBOAT7. The hepatic RNAseq results showed that knockdown of *Mboat7* reduced
317 the expression levels of genes in the liver X receptor (LXR) pathway, suggesting
318 impaired cholesterol excretion (Figure 1K-L). Heatmap analysis further confirmed the
319 downregulation of genes involved in cholesterol excretion (Figure S4C). We then
320 explored how cholesterol excretion is regulated by MBOAT7 and CDS2. Activation of
321 the AMPK pathway is known to inhibit SREBP and enhance LXR protein levels (28).
322 Interestingly, AMPK signaling was downregulated in the liver of sh*Mboat7*, sh*Cds2*,
323 or sh*Mboat7* + sh*Cds2* mice, as indicated by heatmap analysis and western blotting
324 (Figure S4C-E). In contrast, overexpression of *Mboat7* increased p-AMPK and
325 p-ACC levels in *Cds2*$^{f/f}$*;AlbCre* mice, suggesting that AMPK pathway activity was
326 enhanced (Figure 7A-B). This was accompanied by reduced nuclear SREBP2 levels
327 and increased expressions of LXR and its target ABCA1 in *Cds2*$^{f/f}$*;AlbCre* mice
328 (Figure 7A-B). Accordingly, mRNA analysis revealed that downstream targets of
329 LXR (*Abca1*, *Abcg5* and *Abcg8*) were upregulated in the liver of
330 *Mboat7*-overexpressing *Cds2*$^{f/f}$*;AlbCre* mice (Figure S4F). To confirm whether
331 MBOAT7 regulates cholesterol excretion via the AMPK pathway in *Cds2*$^{f/f}$*;AlbCre*
332 mice, we treated primary hepatocytes from *Cds2*$^{f/f}$*;AlbCre* mice with Ad-EGFP and
333 Ad-MBOAT7-EGFP and the AMPK inhibitor dorsomorphin. The results showed that
334 dorsomorphin blocked the ability of *Mboat7* to elevate LXR protein levels (Figure
335 7C). This demonstrates that MBOAT7 regulates cholesterol excretion via the
336 AMPK-LXR axis.

337 We then explored how overexpression of MBOAT7 increases AMPK activity in
338 *Cds2*$^{f/f}$*;AlbCre* mice. Lipolysis regulates key intracellular nutrient-sensing pathways,
339 such as the AMPK pathway (29). Since MBOAT7 overexpression promotes lipolysis
340 in *Cds2*-deficient primary hepatocytes (Figure 6I), we examined this process in
341 primary hepatocytes. Activation of lipolysis with isoprenaline (ISO) enhanced AMPK
342 activity in wild-type primary hepatocytes under both Ad-EGFP and
343 Ad-MBOAT7-EGFP conditions (Figure S4G-H). Conversely, inhibiting lipolysis with
344 the ATGL inhibitor Atglistatin (ATGLi) reduced AMPK signaling (Figure S4I-J),
345 which demonstrates that lipolysis regulates AMPK signaling in primary hepatocytes.

346 In *Cds2*-deficient primary hepatocytes, overexpression of MBOAT7 activated AMPK
347 signaling, which was further enhanced by ISO treatment (Figure 7D-E). Importantly,
348 ATGLi treatment diminished AMPK activation caused by MBOAT7 overexpression
349 in *Cds2*-deficient primary hepatocytes (Figure 7F-G), demonstrating that MBOAT7
350 regulates AMPK activity at least partially by promoting lipolysis. These findings
351 suggest that *Mboat7* reduces LD size and cholesterol content in *Cds2*-deficient
352 conditions by activating the AMPK-LXR axis.
353

354 **Discussion**

355 Here, we elucidate that spatial localization of MBOAT7 to ER-LD contact
356 sites-orchestrated by CDS2-represents a fundamental cellular adaptation to lipid
357 overload. This redistribution is critical for its role in regulating LD dynamics and
358 cholesterol metabolism. At the ER, CDS2 binds to MBOAT7, but in the absence of
359 CDS2, MBOAT7 locates to the ER-LD contacts. This relocation promotes lipolysis
360 and inhibits the targeting of DGAT2 to LDs in a RAB1-dependent manner.
361 Physiologically, MBOAT7-mediated LD size reduction activates the AMPK-LXR axis,
362 enhancing cholesterol excretion (Figure 7H).

363 LDs play an essential role in adaptation to fluctuating metabolic states, through
364 controlling their size, subcellular distribution and interaction with other organelles
365 (30). In response to lipid overload, hepatocytes sequester free fatty acid as triglyceride
366 within the core of LDs to prevent lipotoxicity and oxidative stress. Although the LD
367 size varies considerably across hepatic sinusoids, the physiological relevance of this
368 LD heterogeneity is largely undetermined. LD proteins can integrate nutrient signals
369 and regulate LD size (31), suggesting the existence of an adaptive mechanism that
370 maintains LD dimensions within a degradable range and minimizes lipotoxicity. Our
371 study identifies MBOAT7 and CDS2 as key coordinators of LD size and cholesterol
372 homeostasis. In MASLD mouse livers, MBOAT7 is more concentrated on LDs
373 compared to normal controls, indicating a compensatory redistribution that
374 counteracts steatosis-driven LD expansion. The translocation of MBOAT7 from the
375 ER to ER-LD contacts in the absence of CDS2 depends on RAB1A, consistent with

376 established mechanisms involving Rab GTPases, tethering complexes, and SNAREs
377 in ER-to-LD protein trafficking (18-20).
378 Previous evidence showed that CDS2 deficiency resulted in "supersized" LD. We
379 also observed large LD in *Cds2* deficient hepatocytes (15, 16). We further
380 demonstrate that MBOAT7 expression normalizes LD size in CDS2-KO cells by
381 preventing DGAT2 localization to LDs via a RAB1-dependent mechanism. This
382 process reflects an adaptive response orchestrated by the MBOAT7–RAB1–DGAT2
383 axis to restrict LD expansion. Of note, MBOAT7 antagonizes RAB1-mediated
384 DGAT2 recruitment to LDs. However, this only occurs when CDS2 is absent,
385 suggesting that RAB1 has a stronger binding affinity for DGAT2 than for MBOAT7.
386 Interestingly, GPAT4-mediated LD growth remains unaffected in CDS2 KO cells,
387 highlighting the specificity of this regulatory node.
388 In *Cds2* deficient condition, the compensatory redistribution of MBOAT7 to
389 ER-LD contacts exerts significant physiological effects. It stimulates ATGL-mediated
390 lipolysis, which reduces LD size and elevates cytosolic free fatty acids and cholesterol.
391 Hepatocytes counteract the resulting lipotoxic stress by activating export pathways.
392 We showed that reduced LD size-regulated by ER-LD localized MBOAT7- triggers an
393 energy-consuming futile cycle of triglyceride hydrolysis and resynthesis, raising AMP
394 levels and activating AMPK signaling (29). This in turn enhances fatty acid oxidation
395 and cholesterol excretion, which helps remove toxic free fatty acids and free
396 cholesterol, thereby safeguarding liver health. Given the strong association between
397 MBOAT7 loss-of-function variants and MASLD across various populations (32, 33),
398 therapeutic activation of AMPK may represent a promising strategy for the MBOAT7
399 deficiency-related MASLD.
400 In summary, our findings reveal a previously unrecognized axis of inter-organelle
401 communication and metabolic control, orchestrated by MBOAT7, CDS2, and RAB1
402 that adaptively responds to lipid overload. We demonstrate that LD size directly
403 regulates hepatic cholesterol content through AMPK-LXR signaling, providing a new
404 mechanistic link between organelle membrane dynamics and metabolic homeostasis
405 in MASLD pathogenesis.

406

407 **Material and Methods**

408 **Mice**

409 *Cds2$^{f/f}$* and *Cds2$^{f/f}$;AlbCre* mice were generated as described (16). C57BL/6J mice
410 were purchased from GemPharmatech Co., Ltd. For liver-specific gene knockdowns,
411 C57BL/6J mice were injected with AAV-TBG-sh*Con*, AAV-TBG-sh*Mboat7*,
412 AAV-TBG-sh*Cds2* intravenously (i.v) with $3x10^{11}$ genomic copies of AAVs. The
413 target sequence for *Mboat7* is 5'-CCTGTTGGCTTCCTCTTTAAG-3'. The target
414 sequence for *Cds2* is 5'-GTCCGAAGCAAAGCTAGAT-3'. The control sequence is
415 5'-GAAGTCGTGAGAAGTAGAA-3'. For liver-specific overexpression of *Mboat7*,
416 C57BL/6J mice were injected with AAV-TBG-*Con* or AAV-TBG-*Mboat7*
417 intravenously (i.v) with $1x10^{11}$ genomic copies of AAVs. Mice were housed at room
418 temperature (22°C) and fed a standard rodent chow diet (Beijing HFK Bioscience Co.,
419 Ltd #1032). Unless otherwise stated, 8-week-old male mice were used and all mice
420 were fasted for 5-6 hours prior to euthanization. In some experiments, C57BL/6J mice
421 were fed a chow or GAN diet (Research Diets Inc, D09100310) for 26 weeks. All
422 animal experiments were approved by the Institutional Animal Care and Use
423 Committee (IACUC) at the Institute of Genetics and Developmental Biology, Chinese
424 Academy of Sciences (IGDB-CAS).

425 **Cell culture**

426 The *CDS2* knockout HeLa cell line was generated using the CPISPR/Cas9 system
427 according to published literature (34). The target sequence was
428 5'-TATTTACTGAGAATCCGCAA-3'. HepG2 cells (ATCC, HB-8065) and HeLa
429 cells were cultured in DMEM with 10% FBS. In certain experiments, HeLa cells were
430 transfected with siRNAs. The targeting sequence for RAB1A is
431 5'-CAGCATGAATCCCGAATAT-3'. The targeting sequence for CDS2 is
432 5'-GGCCACCTTTGTCAATGTA-3'. Mouse primary hepatocytes were isolated from
433 *Cds2$^{f/f}$* and *Cds2$^{f/f}$;AlbCre* mice and infected with Ad-EGFP or Ad-MBOAT7-EGFP
434 with MOI=50. All cells were grown at 37°C in a 5% CO_2 incubator.

435 **Plasmids**

436 Human *MBOAT7* cDNA was cloned into the *pcDNA3.1-EGFP* and *pCMV-C-mCherry*
437 vectors. Human *MBOAT5* was cloned into the *pcDNA3.1-EGFP* vector. Human *CDS2*
438 cDNA was cloned into the *pCMV-Tag2b* and *pCS2-HA* vectors. Human *RAB1A*,
439 *DGAT2* and *GPAT4* cDNAs were cloned into both the *pEGFP-N1* and *pCMV-Tag2b*
440 vectors. For His pulldown assays, human *MBOAT7* cDNA was cloned into the
441 *pET-28a* vector.

442 **MBOAT7 activity assay**

443 The activity of MBOAT7 was measured as described with minor modifications (19).
444 Briefly, 100 μg of protein from liver was incubated in 200 μl of medium (10 mM
445 Tris/HCl, pH 7.5, 150 mM NaCl, 1 mM EDTA) with 50 μM lysophosphatidylinositol
446 (LPI), 25 μM arachidonoyl-CoA (20:4-CoA), and 5 μM (0.2 μCi) radiolabeled
447 arachidonoyl[1-14C]CoA. The reaction was incubated for 15-30 minutes at 37 ºC and
448 then stopped by adding 1 mL of chloroform:methanol (2:1, vol/vol) and 0.4 mL of 2%
449 orthophosphoric acid. After centrifugation (3,500 g, 15 min, 4 ºC), the lower organic
450 phase, containing the lipids, was collected and dried under a gentle nitrogen stream.
451 Lipids were reconstituted in chloroform. Total lipids were extracted using the Bligh
452 and Dyer method and separated by one-dimensional TLC on silica gel 60 plates using
453 chloroform/methyl acetate:1-propanol:methanol:0.25% KCl (25:25:25:10:9, vol/vol).
454 The radioactivity in the separated bands were quantified using a Typhoon FLA 9000
455 (GE Healthcare Japan). The corresponding areas of radiolabeled phospholipids on
456 TLC plates were cut out, and the radiolabeled products were measured by liquid
457 scintillation counting.

458 **Lipid analysis**

459 Lipids were extracted based on the chloroform/methanol (2:1, v/v) lipid extraction
460 method (3). In brief, 50 mg of liver tissue were extracted with 6 mL of
461 chloroform/methanol (2:1, v/v), then vortexed and refrigerated overnight. 3 mL of
462 0.043% magnesium chloride was then added to separate the aqueous phase from the
463 chloroform phase which contains the lipids. After separation of the two phases, the
464 upper water/methanol phase was removed. A 0.5-mL aliquot of the bottom phase was
465 combined with 1 mL of 0.5% Triton X-100 in chloroform and dried. Triglyceride and

466 total cholesterol levels were measured using commercially available kits (BioSino,
467 Beijing, China). Plasma free fatty acids (FFA) were measured using commercially
468 available kits (Sigma-Alrich, MAK044).

469 **Immunoprecipitation**

470 Cells were transfected with the indicated plasmids using Lipofectamine 3000
471 (ThermoFisher, L3000001). Proteins were extracted using RIPA lysis buffer,
472 containing100 mM Tris Base, 1% deoxycholate, 0.1% SDS, 5 mM EDTA, 1%
473 Triton-X-100, 150 mM NaCl, pH 8.0), supplemented with 100 mM PMSF, protease
474 inhibitor cocktail (Roche, P8340) and 100 mM sodium vanadate. Lysates were
475 incubated on ice for 15 min, then centrifuged at 12,000 rpm for 15 minutes at 4 °C.
476 Supernatants were incubated overnight at 4 °C with anti-Flag M2 affinity gel
477 (Sigma-Aldrich, A2220) or anti-GPF agarose beads (Lablead Biotech Co., Ltd). After
478 four washes with lysis buffer, beads were denatured in 2X SDS sample buffer for 10
479 min at 100 °C for western blotting. For the pulldown assay, MBOAT7-His was pulled
480 down using Ni-NTA agarose beads (Qiagen, 30210), then washed three times with
481 PBS + PMSF + 1% Triton buffer. 10 μg of *Flag-CDS2* was expressed in 293T cells,
482 immunoprecipitated using anti-Flag M2 affinity gel, and eluted with 3X Flag peptide.
483 The eluted Flag-CDS2 (1.5 mL) was then incubated with the Ni-NTA agarose-bound
484 MBOAT7-His for 2 hours. The immunoprecipitate was washed six times with PBS +
485 PMSF + 1% Triton buffer and denatured with 2X SDS sample buffer for 10 min
486 before western blotting.

487 **Confocal imaging**

488 The images were acquired using a LSM 980 with Airyscan 2 (Zeiss) or a confocal
489 microscope (Leica SP8). Images were analyzed by Image J.

490 **Subcellular fractionation**

491 Subcellular fractionation of liver tissue was performed as described (35).

492 **Antibodies**

493 Rabbit antibodies against CDS2 (1:500, 13175-1-AP), SREBP2 (1:1000,
494 28212-1-AP), LDLR (1:1000, 10785-1-AP), SR-B1 (1:1000, 21277-1-AP) and
495 MBOAT7 (1:100, 83546-3-RR) were purchased from Proteintech. Rabbit antibody

496 against MBOAT7 (1:1000, AV49811) was purchased from Sigma-Aldrich. Mouse
497 antibody against Flag (1:1000, F1804) was purchased from Sigma-Aldrich. Rabbit
498 antibody against Flag (1:2500, PM020) was purchased from MBL. Rabbit antibodies
499 against ATGL (1:1000, 2138), phospho-AMPKα(Thr172)(40H9) (1:1000, 2535),
500 AMPKα (1:1000, 2532), phospho-ACC (1:1000, 3661), ACC (1:1000, 3662), and
501 ABCA1 (1:1000, 96292) were purchased from Cell Signaling. Mouse antibody
502 against LXR (1:1000, ab41902) was purchased from Abcam. Rabbit antibodies
503 against DGAT2 (1:1000, ab237613) and HMGCR (1:1000, ab174830) were
504 purchased from Abcam.

505 **Statistics**

506 Results with error bars are mean±SEM. Comparisons between 2 groups were
507 performed using the two-tailed Student's t-test. ANOVA was used for comparisons
508 between more than 2 groups.

509 **Acknowledgments**

510 We thank Xixian Li from the Center for Biological Imaging at the Institute of
511 Biophysics, CAS, for analyzing images. This work was supported by grants
512 2024YFA1306101, 2023YFA1800500 from National Key R&D Program of China
513 and 92354301, 32230044, 32371230 and 32321004 from the National Natural Science
514 Foundation of China, and BJ-2024-235 from National High Level Hospital Clinical
515 Research Funding.
516 Figure 4A, Figure 6I and Figure 7H were created with BioRender
517 (*https://BioRender.com/ k88h902*, *https://BioRender.com/s73x778, and*
518 *https://BioRender.com/e57c295*).

519 **Declaration of Interests**

520 The authors have declared that no conflict of interest exists.

521 **Author Contributions**

522 J Xu and X Huang designed the experiments. J Xu, J Zhang, W Wang and H Su
523 performed the experiments. J Xu, J Zhang, S Chen and M Ding analyzed the data. J
524 Xu and X Huang wrote the manuscript.

525

526 **References**

527 1. Llovet JM, Willoughby CE, Singal AG, Greten TF, Heikenwälder M, El-Serag HB, Finn RS, et al.
528 Nonalcoholic steatohepatitis-related hepatocellular carcinoma: pathogenesis and treatment. Nature
529 Reviews Gastroenterology & Hepatology 2023;20:487-503.
530 2. Xiang L, Li X, Luo Y, Zhou B, Liu Y, Li Y, Wu D, et al. A multi-omic landscape of steatosis-to-NASH
531 progression. Life Metab 2022;1:242-257.
532 3. Walther TC, Chung J, Farese RV, Jr. Lipid Droplet Biogenesis. Annu Rev Cell Dev Biol
533 2017;33:491-510.
534 4. Schott MB, Weller SG, Schulze RJ, Krueger EW, Drizyte-Miller K, Casey CA, McNiven MA. Lipid
535 droplet size directs lipolysis and lipophagy catabolism in hepatocytes. J Cell Biol 2019;218:3320-3335.
536 5. Buch S, Stickel F, Trepo E, Way M, Herrmann A, Nischalke HD, Brosch M, et al. A genome-wide
537 association study confirms PNPLA3 and identifies TM6SF2 and MBOAT7 as risk loci for alcohol-related
538 cirrhosis. Nat Genet 2015;47:1443-1448.
539 6. Thangapandi VR, Knittelfelder O, Brosch M, Patsenker E, Vvedenskaya O, Buch S, Hinz S, et al.
540 Loss of hepatic Mboat7 leads to liver fibrosis. Gut 2021;70:940-950.
541 7. Varadharajan V, Massey WJ, Brown JM. Membrane-bound O-acyltransferase 7 (MBOAT7)-driven
542 phosphatidylinositol remodeling in advanced liver disease. J Lipid Res 2022;63:100234.
543 8. Alharthi J, Bayoumi A, Thabet K, Pan Z, Gloss BS, Latchoumanin O, Lundberg M, et al. A metabolic
544 associated fatty liver disease risk variant in MBOAT7 regulates toll like receptor induced outcomes. Nat
545 Commun 2022;13:7430.
546 9. Caddeo A, Spagnuolo R, Maurotti S. MBOAT7 in liver and extrahepatic diseases. Liver Int
547 2023;43:2351-2364.
548 10. Liu Y, Wang W, Shui G, Huang X. CDP-diacylglycerol synthetase coordinates cell growth and fat
549 storage through phosphatidylinositol metabolism and the insulin pathway. PLoS Genet
550 2014;10:e1004172.
551 11. D'Souza K, Kim YJ, Balla T, Epand RM. Distinct properties of the two isoforms of
552 CDP-diacylglycerol synthase. Biochemistry 2014;53:7358-7367.
553 12. Moore MP, Wang X, Kennelly JP, Shi H, Ishino Y, Kano K, Aoki J, et al. Low MBOAT7 expression, a
554 genetic risk for MASH, promotes a profibrotic pathway involving hepatocyte TAZ upregulation.
555 Hepatology 2024;81:576-590.
556 13. Tanaka Y, Shimanaka Y, Caddeo A, Kubo T, Mao Y, Kubota T, Kubota N, et al. LPIAT1/MBOAT7
557 depletion increases triglyceride synthesis fueled by high phosphatidylinositol turnover. Gut
558 2021;70:180-193.
559 14. Xu Y, Mak HY, Lukmantara I, Li YE, Hoehn KL, Huang X, Du X, et al. CDP-DAG synthase 1 and 2
560 regulate lipid droplet growth through distinct mechanisms. J Biol Chem 2019;294:16740-16755.
561 15. Qi Y, Kapterian TS, Du X, Ma Q, Fei W, Zhang Y, Huang X, et al. CDP-diacylglycerol synthases
562 regulate the growth of lipid droplets and adipocyte development. J Lipid Res 2016;57:767-780.
563 16. Xu J, Chen S, Wang W, Man Lam S, Xu Y, Zhang S, Pan H, et al. Hepatic CDP-diacylglycerol synthase
564 2 deficiency causes mitochondrial dysfunction and promotes rapid progression of NASH and fibrosis.
565 Sci Bull (Beijing) 2022;67:299-314.
566 17. Helsley RN, Varadharajan V, Brown AL, Gromovsky AD, Schugar RC, Ramachandiran I, Fung K, et al.
567 Obesity-linked suppression of membrane-bound O-acyltransferase 7 (MBOAT7) drives non-alcoholic
568 fatty liver disease. Elife 2019;8.
569 18. Meroni M, Dongiovanni P, Longo M, Carli F, Baselli G, Rametta R, Pelusi S, et al. Mboat7

570 down-regulation by hyper-insulinemia induces fat accumulation in hepatocytes. EBioMedicine
571 2020;52:102658.
572 19. Wang K, Lee CW, Sui X, Kim S, Wang S, Higgs AB, Baublis AJ, et al. The structure of
573 phosphatidylinositol remodeling MBOAT7 reveals its catalytic mechanism and enables inhibitor
574 identification. Nat Commun 2023;14:3533.
575 20. Olarte MJ, Kim S, Sharp ME, Swanson JMJ, Farese RV, Jr., Walther TC. Determinants of
576 Endoplasmic Reticulum-to-Lipid Droplet Protein Targeting. Dev Cell 2020;54:471-487
577 21. Dhiman R, Caesar S, Thiam AR, Schrul B. Mechanisms of protein targeting to lipid droplets: A
578 unified cell biological and biophysical perspective. Semin Cell Dev Biol 2020;108:4-13.
579 22. Pataki CI, Rodrigues J, Zhang L, Qian J, Efron B, Hastie T, Elias JE, et al. Proteomic analysis of
580 monolayer-integrated proteins on lipid droplets identifies amphipathic interfacial alpha-helical
581 membrane anchors. Proc Natl Acad Sci U S A 2018;115:E8172-E8180.
582 23. Bersuker K, Peterson CWH, To M, Sahl SJ, Savikhin V, Grossman EA, Nomura DK, et al. A Proximity
583 Labeling Strategy Provides Insights into the Composition and Dynamics of Lipid Droplet Proteomes.
584 Dev Cell 2018;44:97-112 e117.
585 24. Mejhert N, Kuruvilla L, Gabriel KR, Elliott SD, Guie MA, Wang H, Lai ZW, et al. Partitioning of
586 MLX-Family Transcription Factors to Lipid Droplets Regulates Metabolic Gene Expression. Mol Cell
587 2020;77:1251-1264 e1259.
588 25. Song J, Mizrak A, Lee CW, Cicconet M, Lai ZW, Tang WC, Lu CH, et al. Identification of two
589 pathways mediating protein targeting from ER to lipid droplets. Nat Cell Biol 2022;24:1364-1377.
590 26. Malis Y, Armoza-Eilat S, Nevo-Yassaf I, Dukhovny A, Sklan EH, Hirschberg K. Rab1b facilitates lipid
591 droplet growth by ER-to-lipid droplet targeting of DGAT2. Sci Adv 2024;10:eade7753.
592 27. Wilfling F, Wang H, Haas JT, Krahmer N, Gould TJ, Uchida A, Cheng JX, et al. Triacylglycerol
593 synthesis enzymes mediate lipid droplet growth by relocalizing from the ER to lipid droplets. Dev Cell
594 2013;24:384-399.
595 28. Wang JQ, Li LL, Hu A, Deng G, Wei J, Li YF, Liu YB, et al. Inhibition of ASGR1 decreases lipid levels
596 by promoting cholesterol excretion. Nature 2022;608:413-420.
597 29. Chen G, Zhou G, Lotvola A, Granneman JG, Wang J. ABHD5 suppresses cancer cell anabolism
598 through lipolysis-dependent activation of the AMPK/mTORC1 pathway. J Biol Chem 2021;296:100104.
599 30. Klemm RW, Carvalho P. Lipid Droplets Big and Small: Basic Mechanisms That Make Them All.
600 Annu Rev Cell Dev Biol 2024;40:143-168.
601 31. Bersuker K, Olzmann JA. Establishing the lipid droplet proteome: Mechanisms of lipid droplet
602 protein targeting and degradation. Biochim Biophys Acta Mol Cell Biol Lipids 2017;1862:1166-1177.
603 32. Mancina RM, Dongiovanni P, Petta S, Pingitore P, Meroni M, Rametta R, Boren J, et al. The
604 MBOAT7-TMC4 Variant rs641738 Increases Risk of Nonalcoholic Fatty Liver Disease in Individuals of
605 European Descent. Gastroenterology 2016;150:1219-1230 e1216.
606 33. Xu X, Xu H, Liu X, Zhang S, Cao Z, Qiu L, Du X, et al. MBOAT7 rs641738 (C>T) is associated with
607 NAFLD progression in men and decreased ASCVD risk in elder Chinese population. Front Endocrinol
608 (Lausanne) 2023;14:1199429.
609 34. Ran FA, Hsu PD, Wright J, Agarwala V, Scott DA, Zhang F. Genome engineering using the
610 CRISPR-Cas9 system. Nature Protocols 2013;8:2281-2308.
611 35. Ding Y, Zhang S, Yang L, Na H, Zhang P, Zhang H, Wang Y, et al. Isolating lipid droplets from
612 multiple species. Nat Protoc 2013;8:43-51.

613

614 **Figure Legends**

615 **Figure 1. MBOAT7 and CDS2 regulate lipid metabolism in liver.**

616 (A-B) The correlation between *MBOAT7* and *CDS2* transcript levels in the gene
617 expression datasets GSE48452 (NASH samples) and GSE66676, respectively. (C)
618 The correlation between *MBOAT7* and *CDS2* transcript levels in the GEPIA website.
619 (D-F) Procedure for liver-specific knockdown of *Mboat7* and/or *Cds2* in mice. Mice
620 were injected with AAV-TBG-shCon, AAV-TBG-sh*Mboat7*, AAV-TBG-sh*Cds2*, or
621 AAV-TBG-sh*Mboat7* + AAV-TBG-sh*Cds2* and fed a chow diet for 4 weeks before
622 analysis. (D). Hepatic triglyceride (E) and cholesterol (F) levels were measured in the
623 mice in (D). N=6-7 mice per group. (G) H&E staining of liver sections from mice in
624 (D). Scale bar represents 50 μm in main images and 10 μm in enlarged images. (H)
625 Hepatic steatosis score based on liver sections of mice in (D). N=6-7 mice per group.
626 (I) RNAseq was performed on liver samples from the mice in (D). The numbers of
627 genes up- or down-regulated in sh*Mboat7* vs sh*Con*, sh*Cds2* vs sh*Con* and sh*Mboat7*
628 + sh*Cds2* vs sh*Con* are shown. (J) KEGG analysis results showing the pathways
629 related to the 301 common downregulated genes in (I). (K) qRT-PCR analysis of the
630 mRNA levels of genes that regulate cholesterol and fatty acid metabolism in the liver.
631 N=5-8 mice per group. (L) Western blot analysis of liver lysates from mice in (D).
632 N=3 mice per group. * $p < 0.05$, ** $p < 0.01$, *** $p < 0.001$.

633

634 **Figure 2. MBOAT7 is localized to the ER-LD contacts in CDS2 KO cells.**

635 (A) CDS2 KO and control HeLa cells were transfected with MBOAT7-EGFP and
636 treated with 100 μM OA for 12 hours, followed by LD labeling with LipidTOX. (B)
637 Fluorescence colocalization was analyzed along the white line in the main confocal
638 image. (C) CDS2 KO and control HeLa cells were treated with 100 μM OA for 12
639 hours and immunostained with anti-MBOAT7 antibody. (D) Fluorescence
640 colocalization was analyzed along the white line in the main confocal image. (E) A
641 3D-SIM image reveals that MBOAT7-EGFP enwraps a LD in an OA-treated CDS2
642 KO cell. Scale bar: 2 μm. (F) CDS2 KO and control HeLa cells were transfected with
643 mCherry-SEC61b (an ER marker), then treated with 100 μM OA for 12 hours. LDs

644 were labeled with BODIPY. (G) Fluorescence colocalization was analyzed along the
645 white line in the main confocal image. (H) C56BL/6 mice were fed a chow (control)
646 or GAN (MASLD) diet (40 kcal% fat, 20 kcal% fructose and 2% cholesterol) for 26
647 weeks. Liver sections were immunostained with anti-MBOAT7 antibody. White
648 arrows indicate MBOAT7 enclosing LDs. (I) The number of LDs surrounded by
649 MBOAT7 was quantified by analyzing 1,000 LDs in confocal images. N=9-11 liver
650 sections per group. Except for (E), scale bars represent 10 μm in main images and 2
651 μm in enlarged images.
652
653 **Figure 3. The N-terminus of MBOAT7 is essential for LD targeting of MBOAT7**
654 **and MBOAT7 interacts with CDS2.**
655 (A) Top: 3D structure of MBOAT7 in the ER membrane, highlighting its
656 transmembrane (TM) domains. Bottom: The 11 TM domains of MBOAT7 (boxes)
657 and the three regions of the protein expressed as truncations. (B) CDS2 KO cells
658 transfected with truncated versions of MBOAT7 were treated with 100 μM OA for 12
659 hours, followed by LD labeling with LipidTOX. (C) CDS2 KO cells transfected with
660 MBOAT7-EGFP containing specific TM domain deletions were treated with 100 μM
661 OA for 12 hours. LDs were labeled with LipidTOX. (D) CDS2 KO cells transfected
662 with MBOAT7-EGFP chimeras containing TM3 or TM4 from MBOAT5 were treated
663 with 100 μM OA for 12 hours and labeled with LipidTOX to stain LDs. (E) Co-IP
664 assay showing that Flag-CDS2 precipitates MBOAT7-EGFP. (F) Co-IP assay showing
665 that MBOAT7-EGFP precipitates Flag-CDS2. (G) Co-IP assay demonstrating that
666 endogenous CDS2 precipitates MBOAT7. (H) *In vitro* pull-down assay indicating that
667 Flag-CDS2 directly binds to MBOAT7-His. Scale bars: 10 μm in main images and 2
668 μm in enlarged images.
669
670 **Figure 4. RAB1A is required for targeting of MBOAT7 to LDs in CDS2 KO cells.**
671 (A) Schematic of the workflow for identifying MBOAT7-interacting proteins in
672 control and CDS2 KO cells. (B) Venn diagram illustrating the overlap between the
673 MBOAT7-interacting proteins from (A) and LD proteins from various LD proteomes.

674 (C) Five MBOAT7-interacting proteins identified from the Venn diagram in (B). (D)
675 CDS2 KO cells were transfected with siNC or siRAB1A, and MBOAT7-EGFP, then
676 treated with 100 μM OA for 12 hours. LDs were labeled with LipidTOX. (E) *RAB1A*
677 mRNA levels in HeLa cells transfected with control siRNA or siRAB1A. (F)
678 Quantification of LDs surrounded by MBOAT7-EGFP in control (siNC) or RAB1A
679 knockdown (siRAB1A) cells. (G) Co-IP assay showing that Flag-RAB1A precipitates
680 MBOAT7-EGFP in CDS2 KO cells. (H) Co-IP assay showing that Flag-RAB1A
681 precipitates MBOAT7-EGFP in CDS2 KO cells, and expression of HA-CDS2 in
682 CDS2 KO cells disrupts the RAB1A/MBOAT7 interaction.
683
684 **Figure 5. MBOAT7 reduces LD size in CDS2 KO cells by competing with**
685 **DGAT2 for targeting to LDs.**
686 (A) Control HeLa or CDS2 KO cells were transfected with MBOAT7-EGFP or the
687 MBOAT7(N321A, H356A)-EGFP mutant, then treated with 100 μM OA for 12 hours.
688 LDs were labeled by LipidTOX. Scale bar: 10 μm. (B) Quantification of LD sizes
689 from (A). N=200 per group. (C) 293T cells were transfected with GFP-RAB1A and
690 Flag-DGAT2 or Flag control plasmids. Co-IP assay shows that Flag-DGAT2
691 precipitates GFP-RAB1A. (D) 293T cells were transfected with GFP-RAB1A and
692 Flag-GPAT4 or Flag control plasmid. Co-IP assay shows that Flag-GPAT4 precipitates
693 GFP-RAB1A. (E) CDS2 KO cells were transfected with GFP-RAB1A and
694 Flag-DAGT2 with or without MBOAT7-EGFP. Co-IP shows that Flag-DGAT2
695 precipitates GFP-RAB1A. (F) CDS2 KO cells were transfected with Flag-DGAT2 and
696 GFP-RAB1A with siRNA control (siCon) or siMBOAT7. Co-IP assay shows that
697 Flag-DGAT2 precipitates GFP-RAB1A. (G) Confocal images showing that
698 EGFP-DGAT2 targets to LDs in CDS2 KO cells. MBOAT7-mCherry expression
699 blocks LD targeting of DGAT2. Scale bar: 10 μm in main images and 2 μm in
700 enlarged images. (H) Co-IP assay showing that Flag-DGAT2 precipitates full-length
701 GFP-RAB1A as well as N-terminal and C-terminal truncated forms. (I) Co-IP assay
702 showing that Flag-MBOAT7 precipitates full length GFP-RAB1A as well as
703 N-terminal and C-terminal truncated forms. (J) Co-IP assay showing that

704 Flag-DGAT2 precipitates GFP-RAB1A in CDS2 KO cells treated with or without OA.
705 (K) Co-IP assay showing that Flag-MBOAT7 precipitates GFP-RAB1A in CDS2 KO
706 cells treated with or without OA. **** $p < 0.0001$.
707
708 **Figure 6. MBOAT7 regulates LD size and lipolysis.**
709 (A) MBOAT7 enzymatic activity was measured in *Cds2*$^{f/f}$, *Cds2*$^{f/f}$*;AlbCre* mice, and
710 *Cds2*$^{f/f}$*;AlbCre* mice injected with AAV-TBG-*Cds2*. N=5-6 mice per group. (B)
711 Schematic showing the procedure for hepatic overexpression of MBOAT7 in the liver
712 of mice with and without hepatic depletion of CDS2. *Cds2*$^{f/f}$ and *Cds2*$^{f/f}$*;AlbCre* mice
713 were injected with AAV-TBG-Con or AAV-TBG-*Mboat7* and fed a chow diet for 4
714 weeks before analysis. (C and D) Hepatic cholesterol (C) and triglyceride (D) levels
715 were analyzed in the mice from (B). N=7-8 mice per group. (E) H&E staining of liver
716 sections from *Cds2*$^{f/f}$ and *Cds2*$^{f/f}$*;AlbCre* mice. Scale bar represents 50 μm in main
717 images and 10 μm in enlarged images. (F) Primary hepatocytes isolated from *Cds2*$^{f/f}$
718 and *Cds2*$^{f/f}$*;AlbCre* mice were infected with Ad-EGFP or Ad-MBOAT7-EGFP and
719 treated with 100 μM OA for 12 hours. LDs were stained with LipdTOX before
720 confocal imaging. Scale bar represents 10 μm in main images and 2 μm in enlarged
721 images. (G) Quantification of LD sizes in (F). (H) Western blot analysis of LD, ER
722 and cytosol fractions from the liver of *Cds2*$^{f/f}$*;AlbCre* mice that are injected with
723 AAV-TBG-Con or AAV-TBG-*Mboat7*. (I) Primary hepatocytes from *Cds2*$^{f/f}$ and
724 *Cds2*$^{f/f}$*;AlbCre* mice were infected with Ad-EGFP or Ad-MBOAT7-EGFP, then treated
725 with 10 μM ISO or DMSO (control) for the indicated times. Free fatty acids in the
726 medium were analyzed. * $p < 0.05$, ** $p < 0.01$, *** $p < 0.001$, **** $p < 0.0001$.
727
728 **Figure 7. MBOAT7 and CDS2 regulate cholesterol metabolism through the**
729 **AMPK pathway.**
730 (A) Western blot of *Cds2*$^{f/f}$ and *Cds2*$^{f/f}$*;AlbCre* mice injected with AAV-TBG-Con or
731 AAV-TBG-*Mboat7*, and fed a chow diet for 4 weeks before analysis. (B)
732 Quantifications of proteins from (A). (C) Primary hepatocytes isolated from
733 *Cds2*$^{f/f}$*;AlbCre* mice were infected with Ad-EGFP or Ad-MBOAT7-EGFP. Cells were

734 serum-starved for 4 hours, then treated with 10 μM dorsomorphin in no-glucose
735 DMEM + 10% FBS medium for 4 hours. Western blot analysis was then performed.
736 (D) Primary hepatocytes from *Cds2*$^{f/f}$*;AlbCre* mice were infected with Ad-EGFP or
737 Ad-MBOAT7-EGFP and treated with 10 μM ISO or DMSO (control) for 6 hours.
738 Western blot analysis was then performed. (E) Quantifications of proteins from (D).
739 (F) Primary hepatocytes from *Cds2*$^{f/f}$*;AlbCre* mice were infected with Ad-EGFP or
740 Ad-MBOAT7-EGFP. Cells were pretreated with DMSO (control) or Atglistatin
741 (ATGLi; 20 μM) for 30 minutes, then treated with 10 μM ISO for 6 hours. Protein
742 levels were analyzed by western blotting. (G) Quantifications of proteins from (F). (H)
743 A model illustrating how MBOAT7 and CDS2 regulate LD dynamics and cholesterol
744 metabolism in hepatocytes. CDS2 and MBOAT7 physically interact in the ER
745 membrane and both regulate PI biosynthesis. MBOAT7 catalyzes the generation of
746 PI-AA, which inhibits CDS2 activity. In the absence of CDS2, MBOAT7 relocates to
747 the ER-LD contacts via binding to RAB1. CDS2 deficiency causes increased LD size
748 accompanied by increased recruitment of DGAT2 to LDs, whereas overexpression of
749 MBOAT7 in CDS2-deficient conditions reduces DGAT2 targeting to LDs, increases
750 ATGL recruitment to the LD surface, and reduces LD size. The increased lipolysis
751 induced by MBOAT7 expression activates AMPK, enhancing LXR protein levels and
752 expression of its downstream target genes, thus stimulating cholesterol metabolism. *
753 $p < 0.05$, ** $p < 0.01$, *** $p < 0.001$, **** $p < 0.0001$.

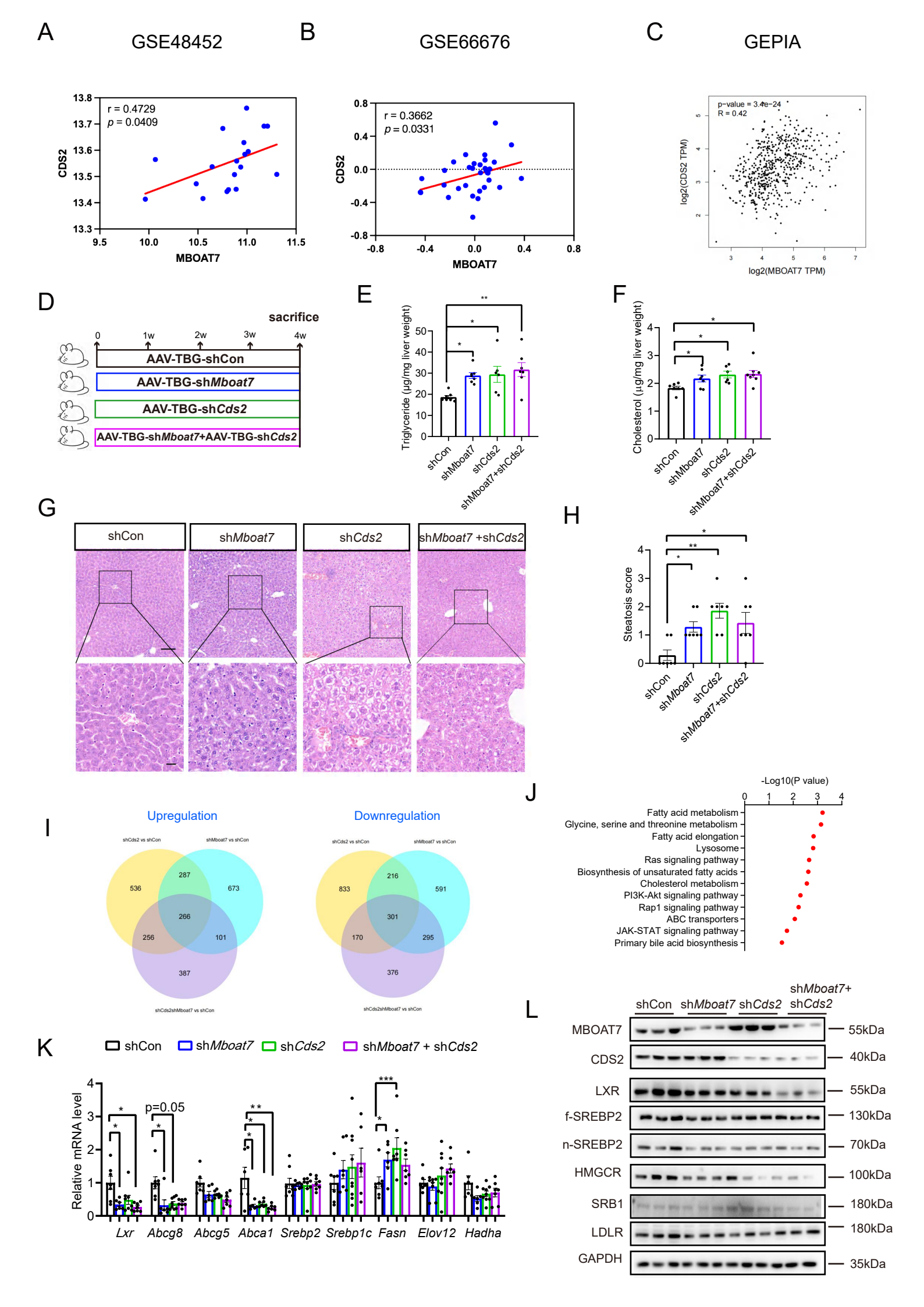
A
GSE48452
r = 0.4729
p = 0.0409
CDS2
MBOAT7
B
GSE66676
r = 0.3662
p = 0.0331
CDS2
MBOAT7
C
GEPIA
p-value = 3.4e-24
R = 0.42
log2(CDS2 TPM)
log2(MBOAT7 TPM)
D
sacrifice
0
1w
2w
3w
4w
AAV-TBG-shCon
AAV-TBG-shMboat7
AAV-TBG-shCds2
AAV-TBG-shMboat7+AAV-TBG-shCds2
E
Triglyceride (μg/mg liver weight)
shCon
shMboat7
shCds2
shMboat7+shCds2
F
Cholesterol (μg/mg liver weight)
shCon
shMboat7
shCds2
shMboat7+shCds2
G
shCon
shMboat7
shCds2
shMboat7 +shCds2
H
Steatosis score
shCon
shMboat7
shCds2
shMboat7+shCds2
I
Upregulation
Downregulation
shCds2 vs shCon
shMboat7 vs shCon
shCds2shMboat7 vs shCon
536
287
673
266
256
101
387
833
216
591
301
170
295
376
J
-Log10(P value)
Fatty acid metabolism
Glycine, serine and threonine metabolism
Fatty acid elongation
Lysosome
Ras signaling pathway
Biosynthesis of unsaturated fatty acids
Cholesterol metabolism
PI3K-Akt signaling pathway
Rap1 signaling pathway
ABC transporters
JAK-STAT signaling pathway
Primary bile acid biosynthesis
K
shCon
shMboat7
shCds2
shMboat7 + shCds2
Relative mRNA level
p=0.05
Lxr
Abcg8
Abcg5
Abca1
Srebp2
Srebp1c
Fasn
Elov12
Hadha
L
shCon
shMboat7
shCds2
shMboat7+ shCds2
MBOAT7
CDS2
LXR
f-SREBP2
n-SREBP2
HMGCR
SRB1
LDLR
GAPDH
55kDa
40kDa
55kDa
130kDa
70kDa
100kDa
180kDa
180kDa
35kDa

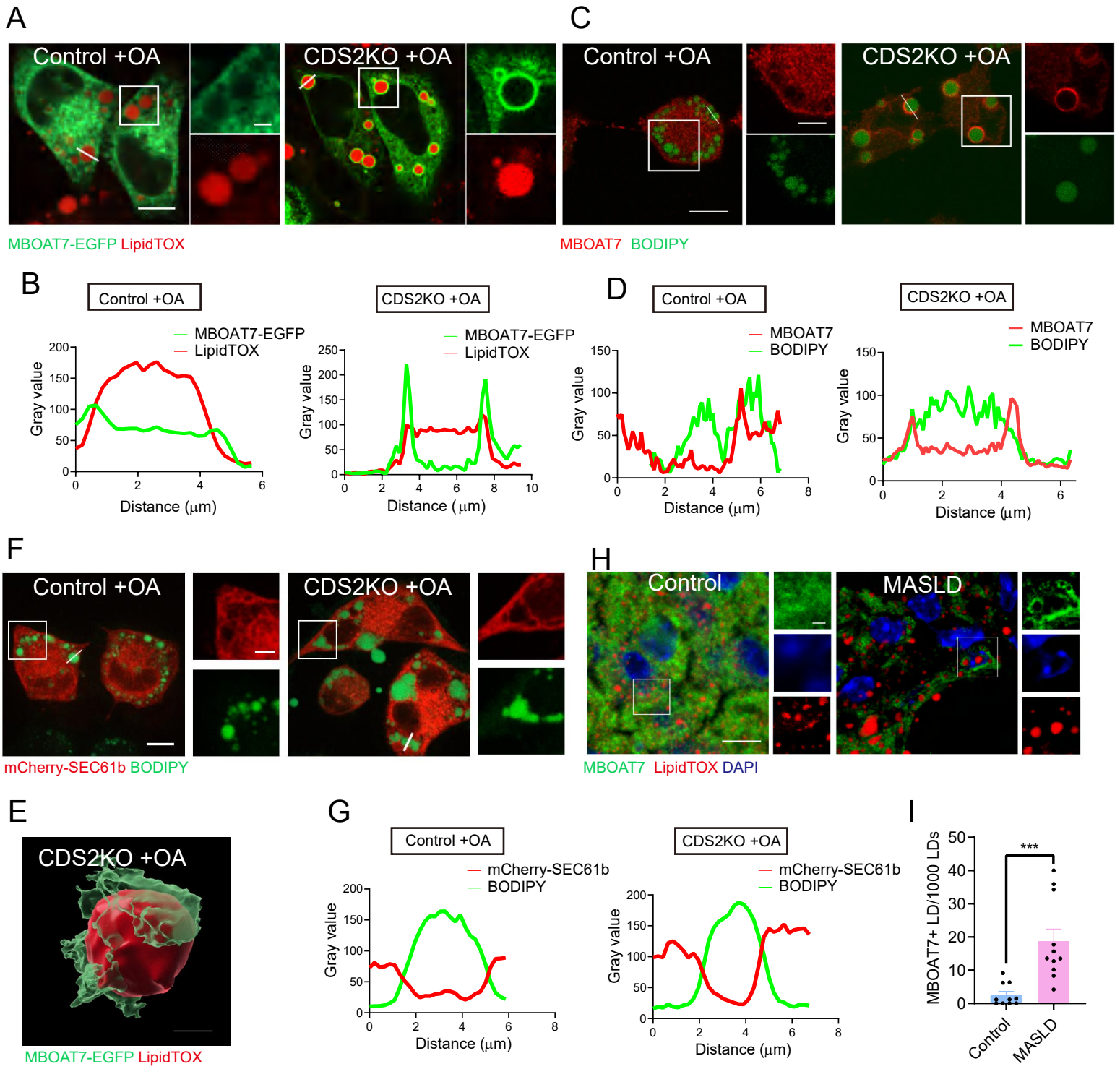
A
Control +OA
CDS2KO +OA
MBOAT7-EGFP LipidTOX
C
Control +OA
CDS2KO +OA
MBOAT7 BODIPY
B
Control +OA
CDS2KO +OA
MBOAT7-EGFP
LipidTOX
Gray value
Distance (μm)
D
Control +OA
CDS2KO +OA
MBOAT7
BODIPY
Gray value
Distance (μm)
F
Control +OA
CDS2KO +OA
mCherry-SEC61b BODIPY
H
Control
MASLD
MBOAT7 LipidTOX DAPI
E
CDS2KO +OA
MBOAT7-EGFP LipidTOX
G
Control +OA
CDS2KO +OA
mCherry-SEC61b
BODIPY
Gray value
Distance (μm)
I
MBOAT7+ LD/1000 LDs
***
Control
MASLD

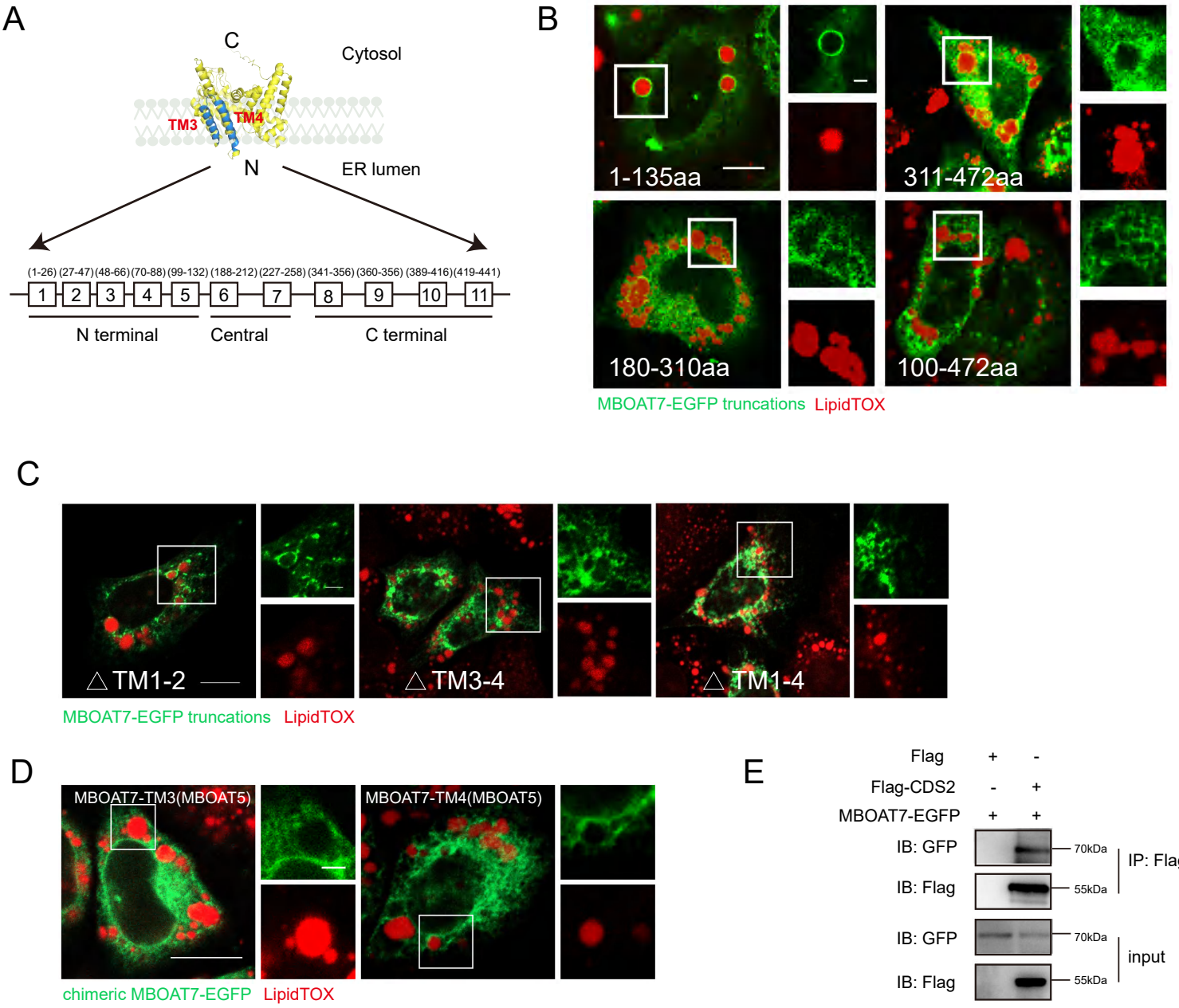
A
C
Cytosol
TM3
TM4
N
ER lumen
(1-26) (27-47) (48-66) (70-88) (99-132) (188-212) (227-258) (341-356) (360-356) (389-416) (419-441)
1 2 3 4 5 6 7 8 9 10 11
N terminal
Central
C terminal
B
1-135aa
311-472aa
180-310aa
100-472aa
MBOAT7-EGFP truncations LipidTOX
C
△TM1-2
△TM3-4
△TM1-4
MBOAT7-EGFP truncations LipidTOX
D
MBOAT7-TM3(MBOAT5)
MBOAT7-TM4(MBOAT5)
chimeric MBOAT7-EGFP LipidTOX
E
Flag + -
Flag-CDS2 - +
MBOAT7-EGFP + +
IB: GFP
IB: Flag
70kDa
55kDa
IP: Flag
input
F
EGFP + -
MBOAT7-EGFP - +
Flag-CDS2 + +
IB: Flag
IB: GFP
55kDa
70kDa
IP: GFP
input
G
Con GFP-CDS2 KI
IB: MBOAT7
IB: GFP
55kDa
70kDa
IP: GFP
input
H
His + -
His-MBOAT7 - +
Flag-CDS2 + +
IB: Flag
IB: His
55kDa
His pulldown
input

A

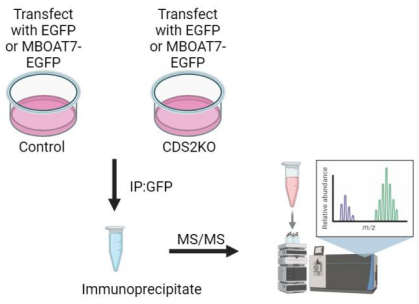

B

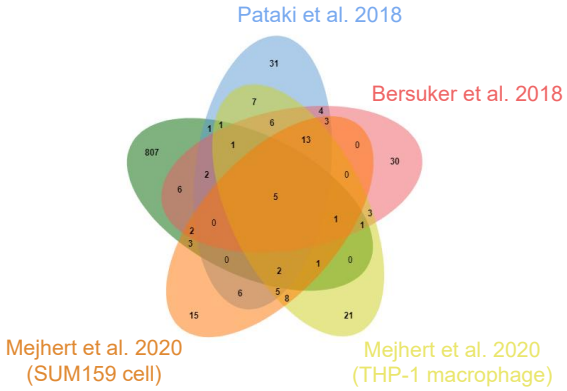

C

Protein	Fold change
RAB7A	10.4
RAB1A	7.2
RAB18	6.2
RAB14	4.8
CYB5R3	4

D

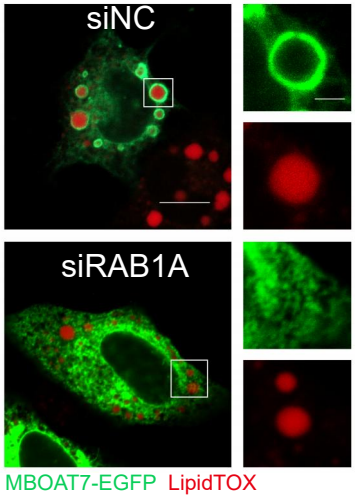

E

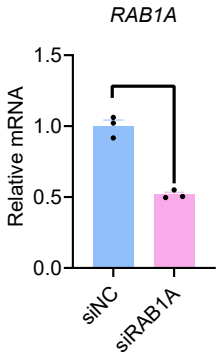

F

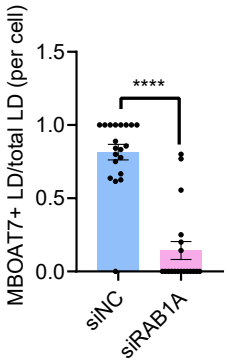

G

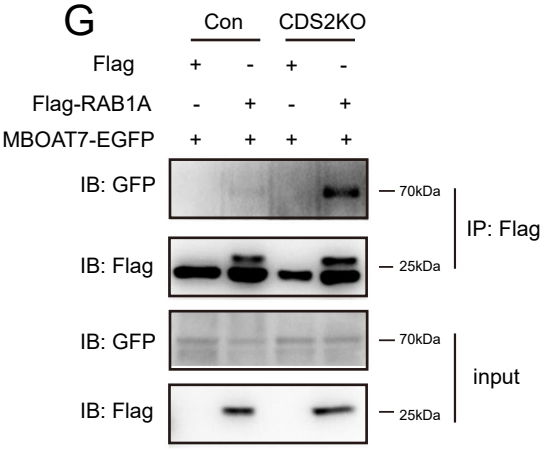

H

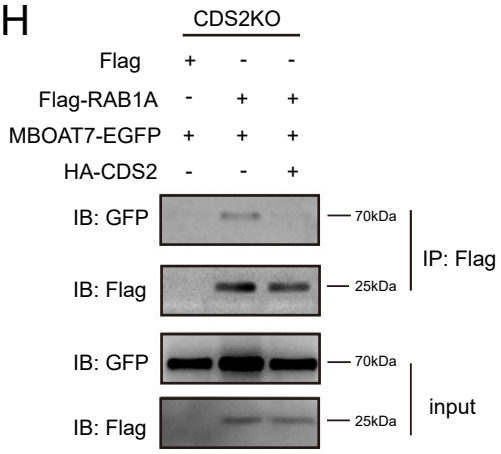

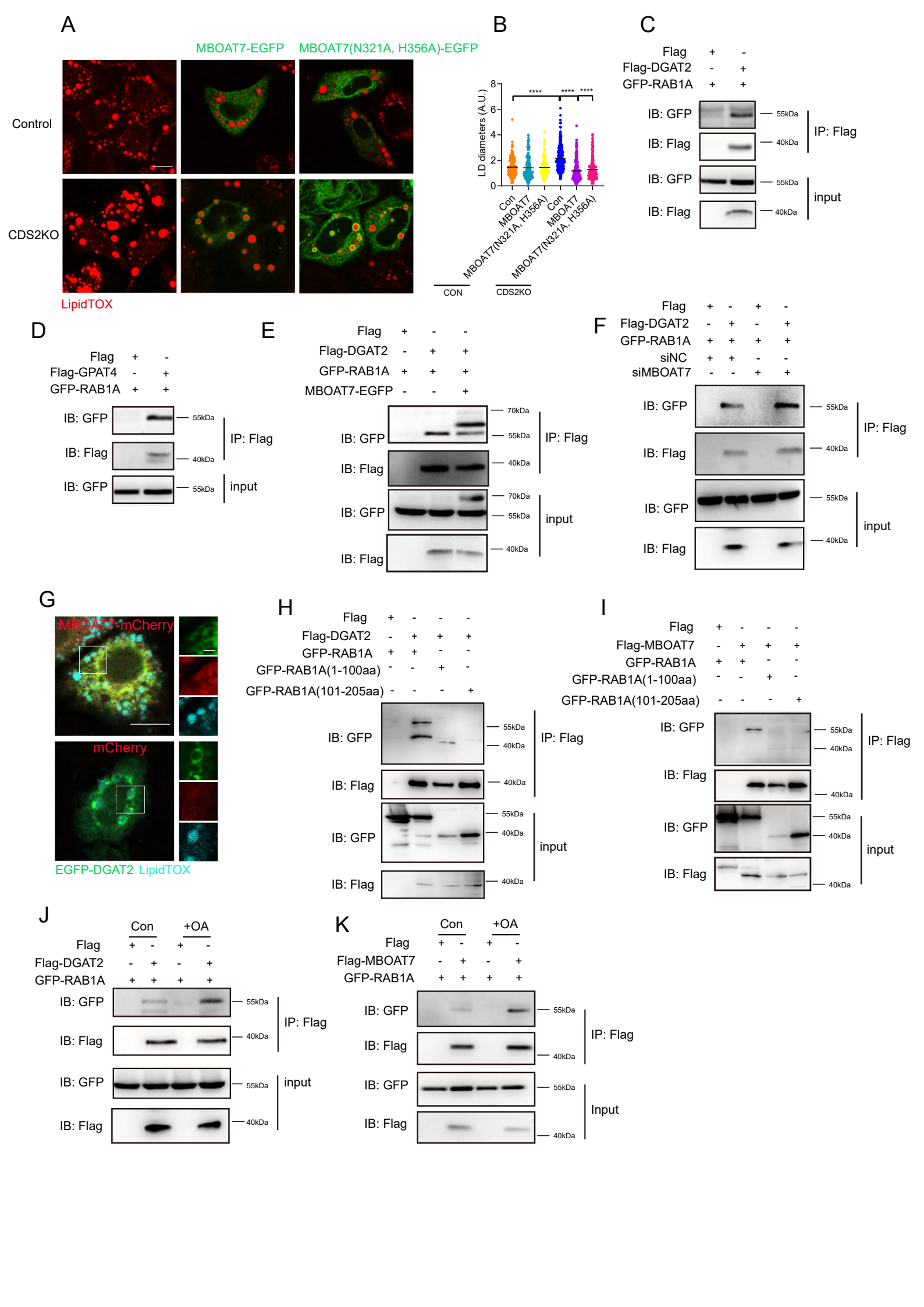
A
MBOAT7-EGFP
MBOAT7(N321A, H356A)-EGFP
Control
CDS2KO
LipidTOX
B
LD diameters (A.U.)
Con
MBOAT7
MBOAT7(N321A, H356A)
CON
CDS2KO
C
Flag
Flag-DGAT2
GFP-RAB1A
IB: GFP
IB: Flag
IP: Flag
input
55kDa
40kDa
D
Flag-GPAT4
E
MBOAT7-EGFP
70kDa
F
siNC
siMBOAT7
G
MBOAT7-mCherry
mCherry
EGFP-DGAT2
LipidTOX
H
GFP-RAB1A(1-100aa)
GFP-RAB1A(101-205aa)
I
Flag-MBOAT7
J
Con
+OA
K
Input

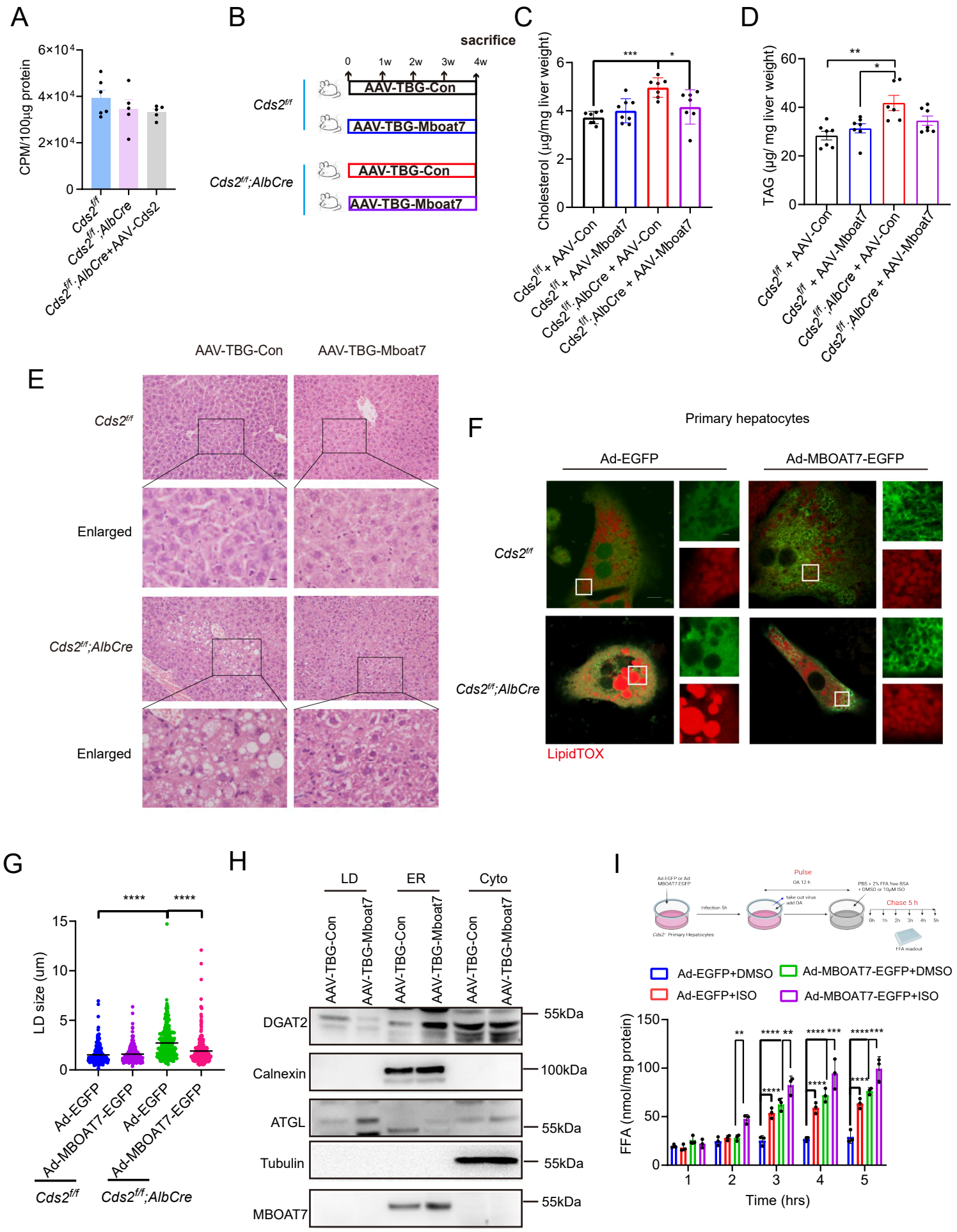
A
CPM/100μg protein
6×10⁴
4×10⁴
2×10⁴
0
Cds2f/f
Cds2f/f;AlbCre
Cds2f/f;AlbCre+AAV-Cds2
B
sacrifice
0
1w
2w
3w
4w
Cds2f/f
AAV-TBG-Con
AAV-TBG-Mboat7
Cds2f/f;AlbCre
AAV-TBG-Con
AAV-TBG-Mboat7
C
Cholesterol (μg/mg liver weight)
***
*
Cds2f/f + AAV-Con
Cds2f/f + AAV-Mboat7
Cds2f/f;AlbCre + AAV-Con
Cds2f/f;AlbCre + AAV-Mboat7
D
TAG (μg/ mg liver weight)
**
*
Cds2f/f + AAV-Con
Cds2f/f + AAV-Mboat7
Cds2f/f;AlbCre + AAV-Con
Cds2f/f;AlbCre + AAV-Mboat7
E
AAV-TBG-Con
AAV-TBG-Mboat7
Cds2f/f
Enlarged
Cds2f/f;AlbCre
Enlarged
F
Primary hepatocytes
Ad-EGFP
Ad-MBOAT7-EGFP
Cds2f/f
Cds2f/f;AlbCre
LipidTOX
G
LD size (um)
****
****
Ad-EGFP
Ad-MBOAT7-EGFP
Ad-EGFP
Ad-MBOAT7-EGFP
Cds2f/f
Cds2f/f;AlbCre
H
LD
ER
Cyto
AAV-TBG-Con
AAV-TBG-Mboat7
AAV-TBG-Con
AAV-TBG-Mboat7
AAV-TBG-Con
AAV-TBG-Mboat7
DGAT2
55kDa
Calnexin
100kDa
ATGL
55kDa
Tubulin
55kDa
MBOAT7
55kDa
I
Pulse
Chase 5 h
Ad-EGFP+DMSO
Ad-MBOAT7-EGFP+DMSO
Ad-EGFP+ISO
Ad-MBOAT7-EGFP+ISO
FFA (nmol/mg protein)
Time (hrs)

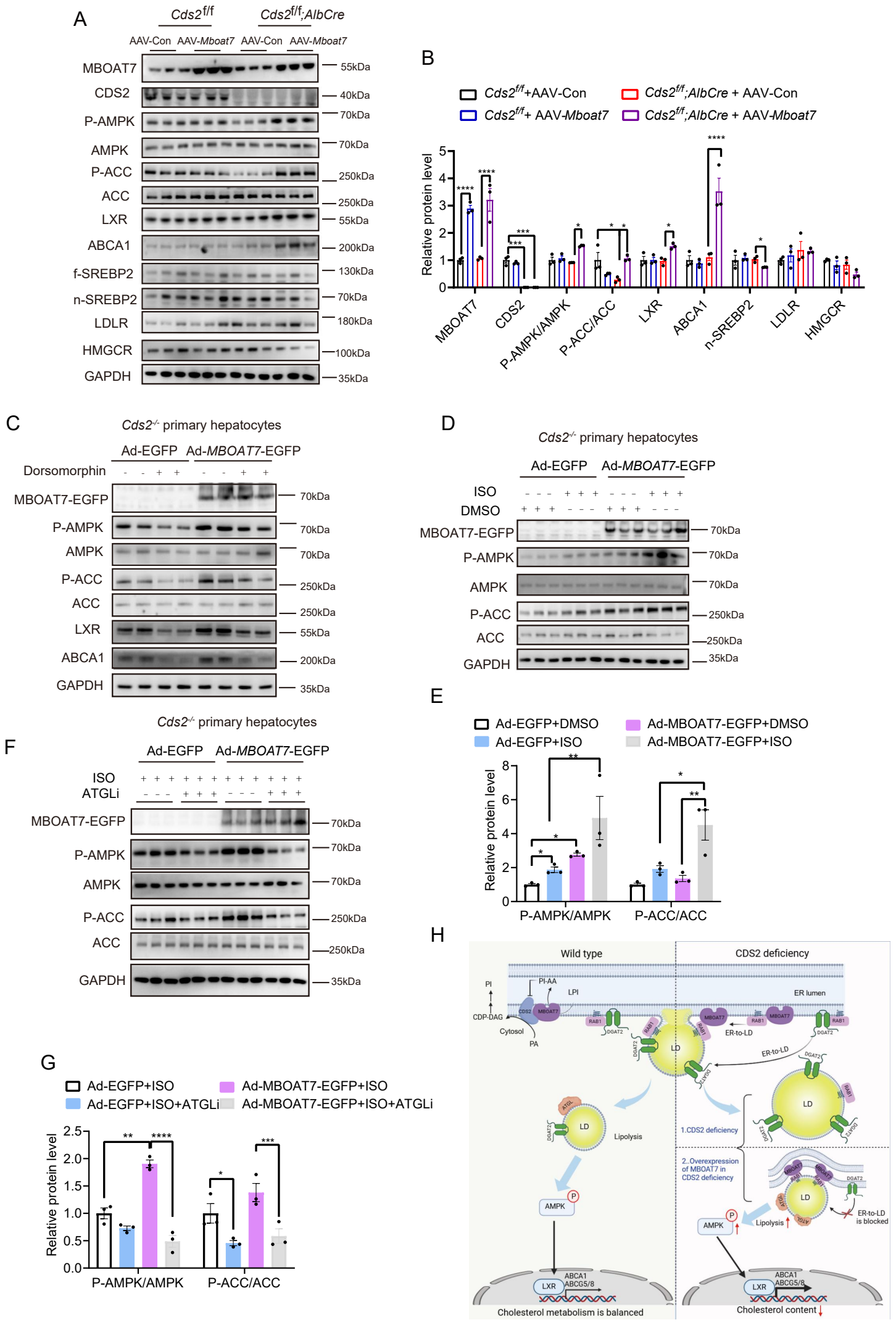
A
Cds2f/f
Cds2f/f;AlbCre
AAV-Con
AAV-Mboat7
AAV-Con
AAV-Mboat7
MBOAT7
CDS2
P-AMPK
AMPK
P-ACC
ACC
LXR
ABCA1
f-SREBP2
n-SREBP2
LDLR
HMGCR
GAPDH
55kDa
40kDa
70kDa
70kDa
250kDa
250kDa
55kDa
200kDa
130kDa
70kDa
180kDa
100kDa
35kDa
B
Cds2f/f+AAV-Con
Cds2f/f+ AAV-Mboat7
Cds2f/f;AlbCre + AAV-Con
Cds2f/f;AlbCre + AAV-Mboat7
Relative protein level
MBOAT7
CDS2
P-AMPK/AMPK
P-ACC/ACC
LXR
ABCA1
n-SREBP2
LDLR
HMGCR
C
Cds2-/- primary hepatocytes
Ad-EGFP
Ad-MBOAT7-EGFP
Dorsomorphin
MBOAT7-EGFP
P-AMPK
AMPK
P-ACC
ACC
LXR
ABCA1
GAPDH
70kDa
70kDa
70kDa
250kDa
250kDa
55kDa
200kDa
35kDa
D
Cds2-/- primary hepatocytes
Ad-EGFP
Ad-MBOAT7-EGFP
ISO
DMSO
MBOAT7-EGFP
P-AMPK
AMPK
P-ACC
ACC
GAPDH
70kDa
70kDa
70kDa
250kDa
250kDa
35kDa
E
Ad-EGFP+DMSO
Ad-EGFP+ISO
Ad-MBOAT7-EGFP+DMSO
Ad-MBOAT7-EGFP+ISO
Relative protein level
P-AMPK/AMPK
P-ACC/ACC
F
Cds2-/- primary hepatocytes
Ad-EGFP
Ad-MBOAT7-EGFP
ISO
ATGLi
MBOAT7-EGFP
P-AMPK
AMPK
P-ACC
ACC
GAPDH
70kDa
70kDa
70kDa
250kDa
250kDa
35kDa
G
Ad-EGFP+ISO
Ad-EGFP+ISO+ATGLi
Ad-MBOAT7-EGFP+ISO
Ad-MBOAT7-EGFP+ISO+ATGLi
Relative protein level
P-AMPK/AMPK
P-ACC/ACC
H
Wild type
CDS2 deficiency
PI
PI-AA
LPI
ER lumen
CDP-DAG
Cytosol
PA
CDS2
MBOAT7
RAB1
DGAT2
LD
ER-to-LD
DGAT1
ATGL
Lipolysis
AMPK
P
LXR
ABCA1
ABCG5/8
Cholesterol metabolism is balanced
1.CDS2 deficiency
2.. Overexpression of MBOAT7 in CDS2 deficiency
ER-to-LD is blocked
Cholesterol content